

Identifying the Role of Electrolyte Additives for Lithium Plating on Graphite Electrode by *Operando* X-ray Tomography

Antoine Klein,^[a] Matthew Sadd,^[a] Nataliia Mozhzhukhina,^[a] Martina Olsson,^[a] Ludovic Broche,^[b] Shizhao Xiong,^[a] and Aleksandar Matic^{*[a]}

The plating of lithium metal on the graphite electrode is a major degradation mechanism in lithium-ion batteries (LIBs). It brings a significant risk of internal short circuit by penetration of dendritic lithium through the separator, leading to short cycle life and safety issues. Understanding how and when plating occurs is crucial for the development of mitigation strategies, e.g. tuning the electrolyte composition. Here we present an *operando* X-ray tomographic microscopy (XTM) study to directly monitor the plating of lithium metal in a lithium/graphite cell. XTM enables a non-destructive and quantitative characterization at *operando* conditions of lithium deposition on a graphite electrode at relevant conditions. In this work it allows us to probe the role of the electrolyte additives vinylene carbonate (VC) and lithium bis(fluorosulfonyl)imide (LiFSI) in the standard LIB electrolyte LP57 (base electrolyte without addi-

tives). The additives show overall better performances in terms of delayed onset of lithium plating which is important for the utilisation of the full capacity of graphite intercalation. We show that there is a transition during lithiation of the dominating mechanism, once lithium plating is initiated this rapidly becomes dominating and hinders further intercalation. For the base electrolyte a homogeneous and dense morphology of plated lithium is found, whereas a more dendritic morphology is observed in the presence of additives. During delithiation, there is a rapid stripping of some of the plated lithium followed by deintercalation. In addition, our work provides a general methodology to track the morphology of plated lithium, which is crucial for fundamental research about battery safety.

Introduction

The success of lithium-ion batteries (LIBs) has its base in the outstanding reversibility of the intercalation reactions taking place at the two electrodes. After the formation of stable interphases, solid electrolyte interphase (SEI) on the anode and cathode electrolyte interphase (CEI) on the cathode, respectively, an exceptional Columbic efficiency underpins a long cycle life. However, following extended cycling or operating under harsh conditions, degradation takes place by e.g. growth of interphases, electrode particle cracking, or binder decomposition.^[1] Lithium plating on the graphite electrode is another major degradation mechanism, especially at high current densities, low temperatures, or overcharging.^[2] Plating lithium instead of intercalating leads to increased electrolyte

consumption by the growth of SEI on the freshly deposited Li metal, risk of formation of dead lithium, i.e., irreversible plating, both leading to loss of active material and capacity fade. Furthermore, lithium plating can form dendrites that eventually pierce through the separator causing internal short circuits and potential thermal runaway in the cell.^[2,3] Some strategies to mitigate lithium plating involve graphite surface modification,^[4] optimised charging,^[5] and tuning the electrolyte formulation.^[6–10] In particular, the use of additives is a common route and it has, for instance, been reported that addition of vinylene carbonate (VC), lithium bis(oxalato) borate (LiBOB), lithium difluoro(oxalato)borate (LiDFOB), or lithium bis(fluorosulfonyl)imide (LiFSI) results in improved SEI and CEI formation.^[6] However, the impedance of the graphite/electrolyte interface is modified through this process, which can impact the plating behavior. For instance, an increased interfacial resistance has been reported with the addition of VC compared to LiFSI, and connected to an increased tendency for plating at low temperature conditions.^[6] Thus, understanding the mechanisms of lithium plating and the role of the electrolyte composition is crucial for increased battery cycle life and safety.

A range of different experimental methods has been applied to characterise lithium plating on graphite anodes, such as optical microscopy, scanning electron microscopy, X-ray and neutron diffraction, electron paramagnetic resonance, and nuclear magnetic resonance.^[11–15] These techniques are normally performed *ex situ*, which means that the sample is analysed

[a] A. Klein, M. Sadd, N. Mozhzhukhina, M. Olsson, S. Xiong, A. Matic
Chalmers University of Technology Department of Physics, 41296 Gothenburg, Sweden
E-mail: matic@chalmers.se

[b] L. Broche
European Synchrotron Radiation Facility, 38000 Grenoble, France

 Supporting information for this article is available on the WWW under
<https://doi.org/10.1002/batt.202400070>

 © 2024 The Authors. *Batteries & Supercaps* published by Wiley-VCH GmbH. This is an open access article under the terms of the Creative Commons Attribution Non-Commercial NoDerivs License, which permits use and distribution in any medium, provided the original work is properly cited, the use is non-commercial and no modifications or adaptations are made.

after cycling. *Operando* experiments offer a deeper insight as they probe processes in a cell while it is being cycled.^[16] X-ray Tomographic Microscopy (XTM) is a non-destructive technique that can provide 3D images on time scales from sub-second to a few minutes,^[17-19] making XTM well suited for battery characterisation.^[16,20] It can provide information on e.g. evolution of electrode morphology, kinetics of processes, degradation mechanisms, or Li-metal plating.^[21] In *operando* XTM, tomograms are collected during battery operation, requiring that the measurement times are short enough to capture the kinetics of the process of interest. Moreover, to be able to differentiate the multiple phases and structures, the resolution should ideally be in the range of a few micrometers or even below. Recently Ho *et al.* observed lithium deposition on a graphite anode under fast-charging conditions using XTM.^[19] They revealed that lithium plating occurred near the separator and had an influence on the lithiation state of the graphite, leading to charge inhomogeneities in the electrode.

In this study, we investigate the effect of electrolyte composition on lithium metal plating on a graphite anode. The electrolyte plays a major role in regulating lithium plating behaviour, which is strongly related to the safety of the battery with respect to e.g. thermal runaway, influencing both the composition and properties of the SEI layer as well as the morphology of plated Li.^[6,7,22,23] Thus, choosing the right salt, solvent and additives is not only crucial for proper Li⁺ transport and cell performance, but will also affect lithium plating. Here we investigate the standard battery electrolyte LP57 (1 M LiPF₆ in a 3:7 wt.% mixture of ethylene carbonate (EC) and ethyl methyl carbonate (EMC)) with the additives vinylene carbonate (VC) and lithium bis(fluorosulfonyl)imide (LiFSI), which are commonly used to regulate the properties of SEI on graphite electrodes. On one hand, VC is known for forming thin polymeric films at the graphite/electrolyte interface protecting the surface from further electrolyte decomposition.^[24] Additionally, VC can be used as a SEI stabilizer against LiPF₆ and increase the thermal stability (thermoreactive electrolyte).^[25] On the other hand, the presence of LiFSI in the electrolyte as an

additive influences the composition and the nature by creating a LiF rich SEI.^[26] It has been suggested that this could lower the SEI resistance on the anode, thus lowering the tendency for lithium plating.^[6] The three investigated electrolytes systems will hereafter be later referred as LP57, LP57+VC and LP57+LiFSI, respectively. We show that electrolyte composition has a direct effect on the morphology of plated lithium, with the observation of mossy lithium and dendritic lithium as well as the formation of dead lithium after delithiation. Quantitative analysis of the *operando* data enables us to determine the onset of lithium metal plating, signaling a switch from the classic intercalation lithium storage mechanism to the undesirable plating mechanism. We show that additives in the electrolyte delay the onset of Li plating until the graphite is close to its fully lithiated state.

Results and Discussion

Figures 1 a and b show the experimental setup for the *operando* tomography experiment, with the two-electrode graphite//lithium half-cell configuration, where 97% of the electrode area is imaged and a full tomogram is recorded during 60 s. In the experiment the current corresponds to a 1C lithiation/delithiation based on the areal capacity of the graphite electrode. Thus, the time scale for taking one tomogram is short enough to provide a representative image of the electrode at a certain state of charge/discharge. A typical voltage profile during an *operando* experiment is shown in Figure 1c. One can note that the cell voltage falls below 0 V which in certain cases can indicate plating of lithium. However, due to the cell configuration an increased overvoltage can be expected as the result of a high IR drop in the *operando* cell and in addition due to high lithium electrode polarisation due to the relatively high current densities ($\sim 3 \text{ mA/cm}^2$) passed through the lithium counter/reference electrode.^[27] Thus, in this experiment, and generally in two-electrode set-ups, the plating of lithium cannot be identified directly from the voltage profile.

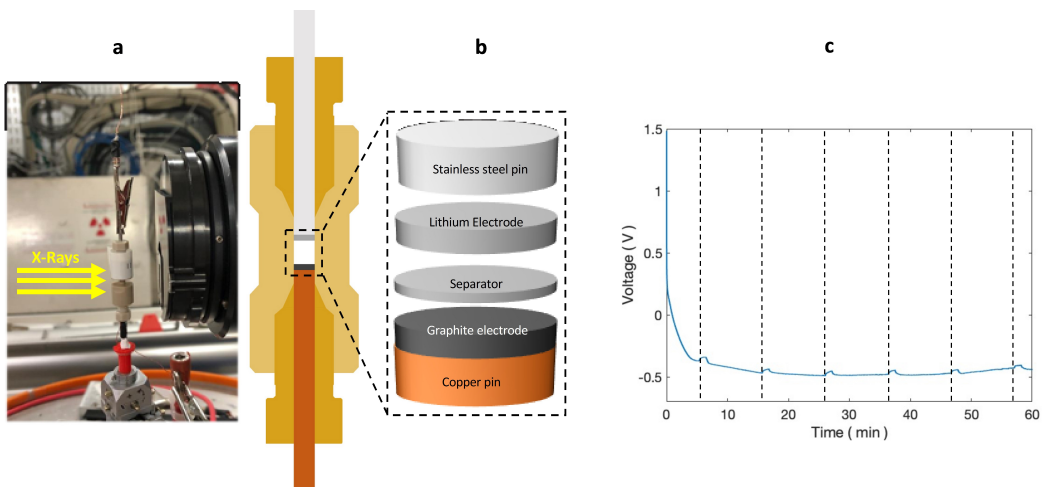


Figure 1. a) Experimental setup for operando tomography, b) Schematic of operando tomography cell and cell components, c) Voltage profile during galvanostatic lithiation of the graphite electrode in LP57 electrolyte. Vertical dashed lines indicate where tomograms were taken.

Figure 2 shows the results from the *operando* tomography experiment with the LP57+VC electrolyte. XTM experiments were performed at static conditions (OCV) before and after lithiation/delithiation, whereas *operando* measurements were performed during cycling. An illustration of how vertical slices were extracted from the full volume rendering is shown in Figure S1. The graphite phase can be observed as grey particles (approximate size 10 µm) in the bulk electrode whereas plated Li appears as a black phase, due to the lower electron density, at the interface between the electrode and the separator. After lithiation for one hour plated Li, with a dendritic morphology with a height of up to 45 µm, can be identified between the graphite electrode and the glass fibre separator, by comparing images from the pristine electrode (Figure 2c) and after lithiation (Figure 2b,g). What is referred to as “pristine” electrode in Figure 2c (and Figures S2c and S3c) is the electrode prior to the *operando* experiment but after three slow formation cycles, see methods section. From the time series of tomo-grams, we can follow the development of the electrode morphology. In the first 25 minutes (Figure 2d) no real changes can be observed to morphology apart from an increase in electrode thickness (see further below) resulting from the intercalation process. From 30 minutes into lithiation, the onset of lithium plating at the electrode/separator interface can be observed (Figure 2e), at this point the potential is also below 0 V. With further lithiation growth of dendritic structures of plated Li is observed on top of the graphite electrode (Figure 2f). In the following delithiation step (Figures 2 h, i) there is initially a rapid decrease of the plated Li phase. However, at the end of delithiation plated Li can still be identified showing that only a part has been stripped and that we have the formation

of dead lithium (Figure 2j). The tomography cross sections in Figure 2 suggest that most of the plated Li is stripped in the initial 5 minutes of the delithiation process. This can be directly correlated to the end of the first plateau in the voltage profile suggesting that stripping of metallic lithium and deintercalation of graphite take place sequentially, which would be in agreement with previous results from differential capacity analysis.^[6]

Figure 3 compares reconstructed vertical slices after lithiation and delithiation of graphite electrodes cycled in the three different electrolytes. Slices from the time series of cycling with the LP57 and LP57+LiFSI electrolytes and the corresponding voltage profiles are shown in Figures S2 and S3. Similarly, to the behaviour found for the electrolyte with VC as additive, also for the electrolyte with the addition of LiFSI, one can observe plated Li at the electrode/separator interface throughout the cell. In this case, both a tall dendritic phase and lower deposits can be identified. Also, for the graphite electrode cycled with the base electrolyte (Figure 3a) Li plating is found after lithiation. However, the plated Li at the graphite/separator interface appears more homogenous and thinner (approximately 10 µm). The morphology is clearly not dendritic, but can be identified as mossy Li, which is in agreement with previous results in literature at similar operating conditions and for a similar electrolyte.^[19] One can note that the lithiation step for the cell with the base electrolyte finished after 40 minutes (compared to one hour for the other cells) when it reached the cut off voltage. However, the amount of plated Li is at this stage very similar to the other cells after plating for one hour, see further below, thus a direct comparison of the morphologies post plating is still valid.

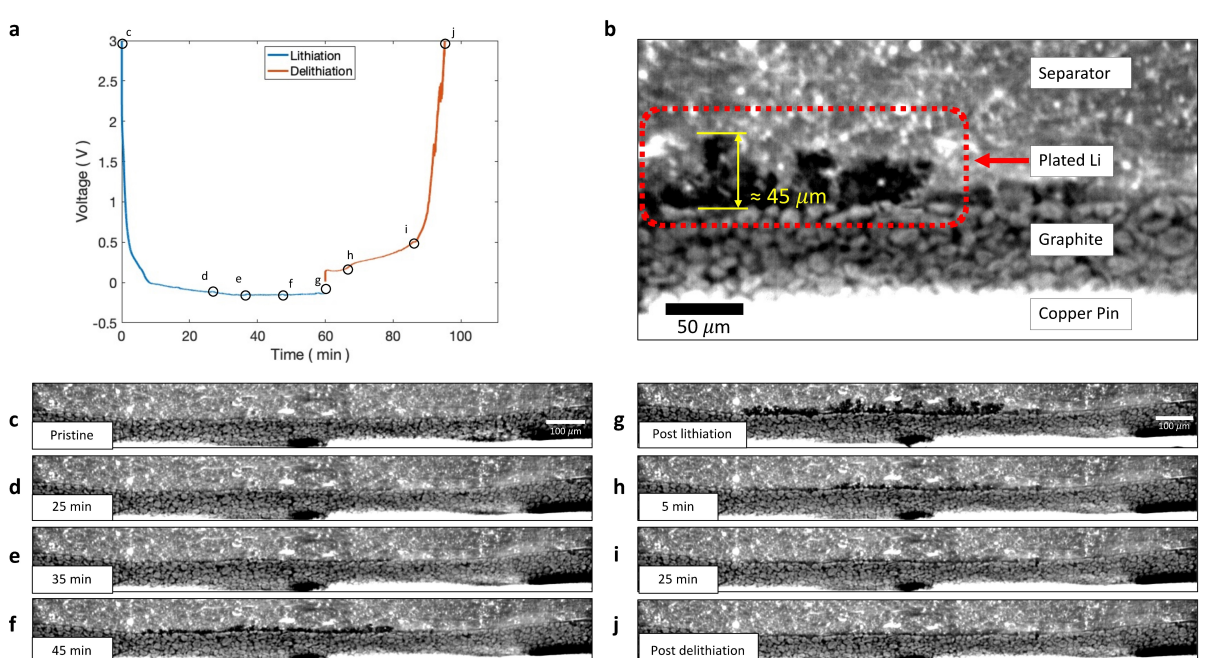


Figure 2. Data from *operando* tomography experiment with LP57+VC electrolyte. a) Voltage profile during graphite lithiation/delithiation at 1 C with circles indicating when tomograms were taken. b) Zoomed in reconstructed vertical slice after lithiation for one hour. Cell components are indicated together with the identification of plated Li. Reconstructed vertical slices during lithiation (d–f) and delithiation (h–i). Tomograms of the pristine electrode, post plating and post stripping (c, g, j) were taken at open circuit voltage.

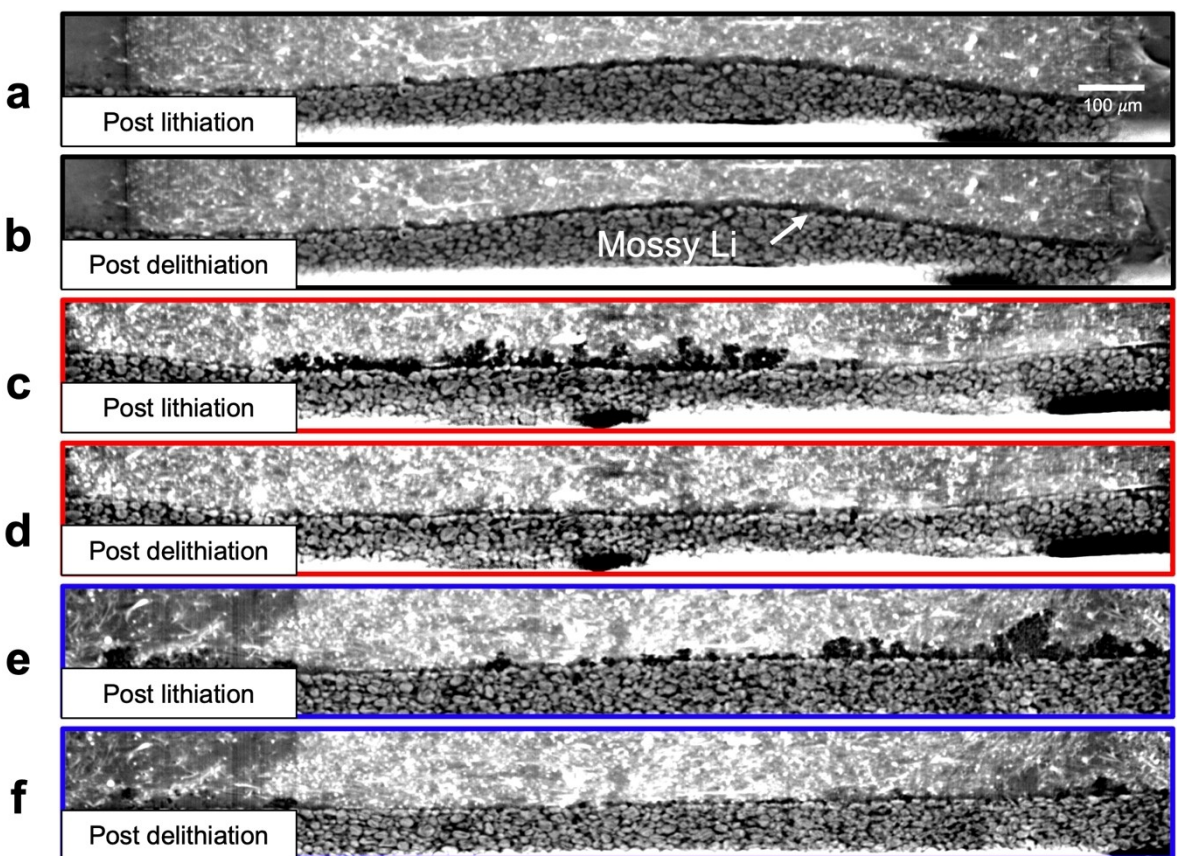


Figure 3. Reconstructed vertical slices from tomograms at the end of lithiation/delithiation of electrodes cycled in LP57 (a,b, black frames), LP57 + VC (c,d, red frames) and LP57 + LiFSI (e,f, blue frames) electrolytes.

During the delithiation process, the plated Li on all three graphite electrodes is partly stripped and dead lithium is left after the cells have polarized (Figure 3b, d and f). One can note that the dendritic structures observed in the presence of the additives VC and FSI after lithiation are to a large extent reversible. It is worth mentioning that the cell with base

electrolyte shows an early polarization to cutoff voltage during delithiation, despite the homogenous morphology of deposited Li.

To further visualize the morphology of plated Li and its distribution over the electrode surface, height maps are shown in Figure 4. These maps show the height of segmented plated

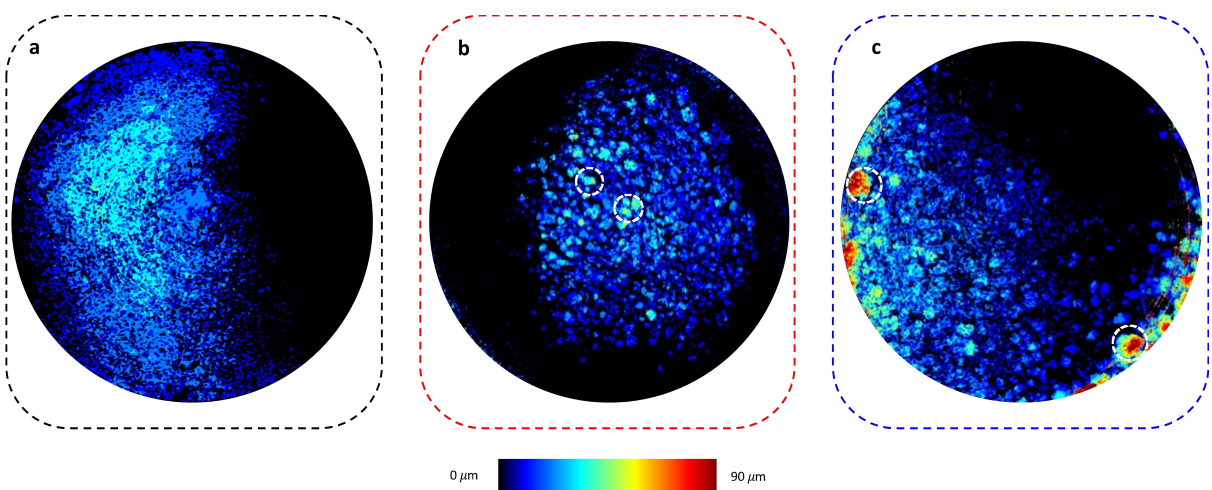


Figure 4. Height map of plated Li in a) LP57 b) LP57 + VC and c) LP57 + LiFSI electrolytes. Segmented surfaces represent 60% of the cell area. The graphite surface (interface between graphite and separator/Li microstructures) is represented in black. White circles highlight lithium dendrites.

Li in each pixel above the graphite electrode surface, providing a 2D representation of the morphology. For the electrode cycled in LP57, finely grained deposits are found, whereas for the electrodes cycled in LP57 + LiFSI and LP57 + VC, more coarse, granular, deposits can be observed, with local areas of taller dendritic structures (highlighted by white circles). This underlines the increased tendency of a dendritic morphology for Li-plating when VC or FSI are added to the electrolyte.

To quantify the changes during lithiation, Figure 5 shows the change in electrode thickness determined from vertical 2D slices (see Figure S4) and the volume of segmented lithium on the graphite electrode/separators interface. It has previously been reported that graphite undergoes an expansion of 10–13% when fully lithiated.^[19,28–30] For the electrodes cycled in LP57 + VC and LP57 + FSI, respectively, the total thickness change is in line with previous reports. The thickness increase starts at the beginning of lithiation and the maximum thickness is reached after 50 minutes, i.e. close to the theoretical capacity of the graphite electrode. In contrast, Li plating is only detected after 20–30 minutes into lithiation. Thus, we observe a transition of dominating mechanism from insertion to plating around this point. For the LP57 + VC electrolyte, in particular, the transition between insertion and plating is rather abrupt. For the LP57 base electrolyte a different behavior is observed, with a considerably smaller increase in thickness and plating occurring in parallel with insertion from the start and becoming the dominating electrochemical process already after 20 minutes. Thus, the graphite is in this case not fully lithiated when plating starts, as is seen by the considerably smaller increase in electrode thickness which levels off at a quite early stage. Thus, the plating effectively terminates insertion into graphite at an early stage.

During delithiation, an initial rapid decrease in the volume of plated Li is observed. Thus, the preferential mechanism for delithiation is initially stripping of metallic lithium in all three cases. The decrease in electrode thickness is instead more gradual. At the end of delithiation we find that only half of the plated Li has been stripped LP57 + FSI, whereas it is fully stripped in LP57 + VC. The opposite trend is found for the electrode thickness with a fully reversible change in the case of LP57 + FSI and irreversible thickness change for the electrode

cycled in LP57 + VC before cell polarization. Thus, the limited reversibility, i.e. the decrease in the coulombic efficiency, has different origin in these two cases, the formation of dead lithium from plating and irreversible intercalation for electrolytes with LiFSI and VC, respectively. One should note that the cell with the LP57 electrolyte polarizes early during delithiation which can be linked to the low degree of Li insertion in graphite. Thus, firm conclusions on which of the processes, delithiation of graphite and stripping of plated Li, that is the limiting step cannot be firmly drawn. After polarization of the cell, a small increase can be observed, but this increase is within the accuracy of experiment and not a real effect.

It is clear that the additives used in this study change the influence of Li plating, both in terms of onset and in terms of morphology. For the base electrolyte the homogeneous plating effectively seems to block access to graphite for Li-ions, which are instead preferentially plated. The additives used in this study are SEI modifiers, and with this modified SEI a delay of plating is found, allowing intercalation to proceed further. The nature of the SEI formed with the two additives should be different, which potentially can be correlated to the difference in behavior. With VC, the SEI will include a polymer sacrificial layer, whereas with LiFSI more inorganic compounds, such as LiF are included in the SEI.^[24,26] One should note that the SEI will not only form on the graphite but also on the freshly plated Li and that this also influences the morphology and reversibility of the plated Li.

Conclusions

A synchrotron-based *operando* X-ray tomography is employed to track potential plating of lithium on graphite electrodes, identifying the morphology evolution of plated Li and the correlation of plated Li to electrolyte composition. With the dedicated *operando* tomography full cell, tomograms can be acquired in 60 s, which is fast enough to capture morphology changes of the electrode and plated Li at a rate of 1C. Our results show that the morphology of plated Li is highly dependent on the composition of the electrolyte. With the additives, VC and LiFSI, a delayed onset for Li-plating is

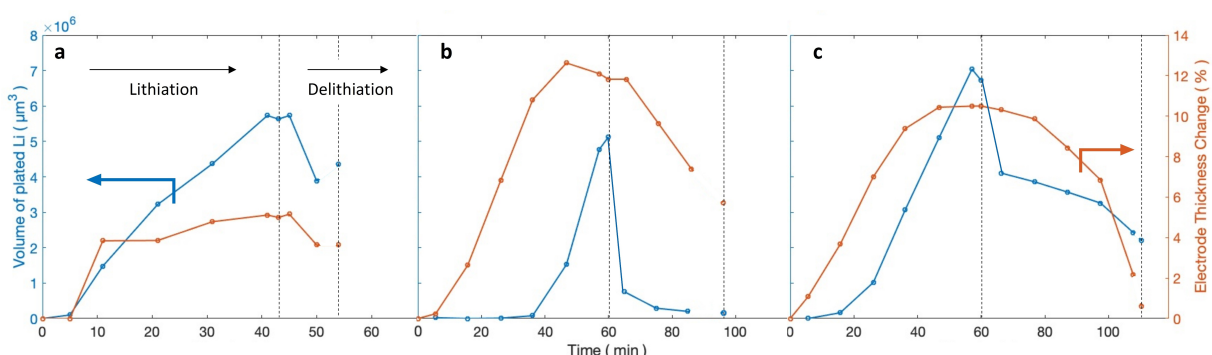


Figure 5. Volume of segmented plated lithium and electrode thickness change with respect to thickness of the pristine electrode for electrodes cycled in a) LP57 b) LP57 + VC and c) LP57 + LiFSI electrolytes. Dashed lines indicate data from tomograms taken at OCV between lithiation/delithiation and after delithiation.

observed compared to the baseline electrolyte LP57. While for the base electrolyte plating and lithiation of graphite start almost simultaneously, Li plating is observed only around halfway into lithiation in the presence of additives. In all three cases once Li-plating starts it rapidly becomes the dominating lithiation mechanism. We also observe a difference in the plated morphology. The plated Li in the base electrolyte shows a rather homogeneous, dense, mossy morphology, whereas in the presence of the additives a dendritic morphology is found. At delithiation, there is a rapid stripping of part of the plated Li and the formation of dead Li is also found on the graphite electrode/separator interface. The limiting factor for the reversibility is different for the two additives. With VC the plated Li is almost fully stripped, whereas the graphite is not fully delithiated. For LiFSI the situation is the opposite with substantial amount of dead Li found and the intercalation of graphite being almost fully reversible.

Methods

Electrolyte Preparation

LP57, 1 M lithium hexafluorophosphate in ethylene carbonate and ethyl methyl carbonate (3:7 wt.%), and LP57 with 2 wt.% vinylene carbonate (VC) were purchased from E-Lyte Innovations. LP57 with 0.1 M lithium bis(fluorosulfonyl)imide (LiFSI, E-Lyte Innovations), corresponding to 1.6 wt.%, was prepared using a 10 mL volumetric flask, by mixing LiFSI and LP57. All components were used as received and possess purity >99% with H₂O content <20 ppm and HF content <50 ppm.

Cell Fabrication

An electrochemical cell for *operando* X-ray tomographic microscopy was built using a polyether ether ketone (PEEK) union with a 1.59 mm internal diameter (VICI). Electrodes were placed on a stainless-steel pin (1.59 mm in diameter). The composite graphite electrode was manufactured by CIDITEC using the following composition: 15–4 Graphite (IMERYS), 94 wt%; C45 Carbon Black (IMERYS), 2 wt%; BM451B SBR (ZEON), 2 wt%; Carboxymethyl cellulose binder: Walocel CRT2000(DOW), 2 wt%. The thickness of the electrode coating given by the manufacturer is 73 µm with an areal capacity of 3.3 mAh/cm². The graphite electrode was punched to a diameter of 1.5 mm and used as the working electrode. Li foil (Honjo Metals) was used as the Li counter electrode. A 1.5 mm piece of glass fibre (Whatman) was used as the separator. Cell assembly was performed in an argon-filled glovebox. A stainless-steel pin with Li was first pushed into the cell and held in place by the casing's compression fitting assembly. The separator was added and 20 µL electrolyte was added into the cell. Finally, the graphite electrode was placed in the cell and the second stainless-steel was pushed in and sealed in place.

Electrochemical Formation Cycles Protocol

The following formation cycles protocol was performed within the *operando* tomography cell in our laboratory before transportation: 6 hours at OCV and three cycles of Constant Current Constant Voltage (CCCV) with C/10 lithiation constant current step with a cut-off of 0.01 V and a constant voltage step at 0.01 V until a current cut-off below C/50, followed C/10 delithiation to 3 V.

Formation cycles were performed on a Scriber Associates 580 battery cycler. The cells were then packed and sealed under argon atmosphere. An overview of the different voltage profiles during formation cycles is shown in Figure S5.

Operando Synchrotron X-ray Tomographic Microscopy

Operando X-ray tomographic microscopy experiments were performed at the ID19 Beamline at the European Synchrotron Radiation Facility (ESRF), Grenoble, France. The X-ray energy was 26.5 keV (pink beam). Tomograms were acquired by a PCO.Edge 5.5 camera (2560x2160 pixels), when using a x20 objective a 0.332 µm voxel size was achieved. A half-acquisition method was applied to provide a field of view of 1.48 mm×0.70 mm. With an electrode area of 1.5 mm, 97 % of the electrode was within the field of view. Tomograms were constructed from 4000 projections equally distributed over 360 degrees, with an exposure time of 15 ms per projection, giving a measurement time of 60 s, not including flat and dark fields taken before and after each measurement. Tomographic reconstructions were performed using the beamlines implementation of the TomoPy software package.

For *operando* XTM, cells were cycled with a Biologic SP300 potentiostat at the beamline. XTM measurements were made before cell cycling and *operando* XTM was made 5 minutes into each cycling step and then made every 10 minutes thereafter. A final XTM measurement was made after each cycling step.

Analysis of Tomograms

Tomograms were analysed with the software Avizo. All tomograms are shown without any noise filtering or image filtering to keep them as close to the raw data. Segmentation of the plated lithium was done with the interactive thresholding tool on a cropped cylindric volume (1151 µm diameter×87.3 µm height) with a surface covering up to 60 % of the field of view. Electrode height measurements were performed with the measurement tool in Avizo for every scan on multiple positions across graphite electrode (see Figure S4). Height maps were produced in MATLAB (MathWorks, Inc.) with the colour bar based on the tallest dendritic microstructure observed.

Acknowledgements

This project has received funding from the European Union's Horizon 2020 research and innovation programme under grant agreement No 957189. The project is part of BATTERY 2030+, the large-scale European research initiative for inventing the sustainable batteries of the future. The project is also supported through the VINNOVA competence centre BASE.

We also acknowledge CIDITEC for providing graphite electrodes within the BIGMAP project.

Conflict of Interests

The authors declare no conflict of interest.

Data Availability Statement

The data that support the findings of this article are available from the corresponding author upon request.

Keywords: Li plating • graphite • Li-ion batteries • X-ray tomography • *operando*

- [1] X. Lin, K. Khosravinia, X. Hu, I. Li, W. Lu, *Prog. Energy Combust. Sci.* **2021**, *87*, 100953.
- [2] D. Hu, et al., *Chin. J. Chem.* **2021**, *39*, 165–173.
- [3] Y. Li, et al., *ACS Appl. Mater. Interfaces* **2019**, *11*, 46839–46850.
- [4] K. R. Tallman, et al., *ACS Appl. Mater. Interfaces* **2019**, *11*, 46864–46874.
- [5] T. Waldmann, M. Kasper, M. Wohlfahrt-Mehrens, *Electrochim. Acta* **2015**, *178*, 525–532.
- [6] J. P. Jones, Smart, C. Marshall, F. C. Krause, R. V. Bugga, *J. Electrochem. Soc.* **2020**, *167*, 020536.
- [7] Q. Q. Liu, R. Petibon, C. Y. Du, J. R. Dahn, *J. Electrochem. Soc.* **2017**, *164*, A1173–A1183.
- [8] S. Tu, et al., *Nat. Energy* **2023**, *8*, 1365–1374.
- [9] X. Xu, X. Yue, Y. Chen, Z. L. Liang, *Angew. Chem. Int. Ed.* **2023**, *62*, e202306963.
- [10] X. Yue, et al., *Angew. Chem. Int. Ed.* **2023**, *62*, e202302285.
- [11] V. Zinth, et al., *J. Power Sources* **2014**, *271*, 152–159.
- [12] W. Mei, et al., *Energy Storage Mater.* **2024**, *66*, 103193.
- [13] B. Ma, S. Agrawal, R. Gopal, P. Bai, *ACS Appl. Mater. Interfaces* **2022**, *14*, 54708–54715.
- [14] J. Wandt, P. Jakes, J. Granwehr, R. A. Eichel, H. A. Gasteiger, *Mater. Today* **2018**, *21*, 231–240.
- [15] D. P. Finegan, et al., *Energy Environ. Sci.* **2020**, *13*, 2570–2584.
- [16] P. Pietsch, V. Wood, *Annu. Rev. Mater. Res.* **2017**, *47*, 451–479.
- [17] M. Di Michiel, et al., *Rev. Sci. Instrum.* **2005**, *76*, 043702.
- [18] R. F. Ziesche, et al., *Nat. Commun.* **2020**, *11*, 1–11.
- [19] A. S. Ho, et al., *ACS Nano* **2021**, *15*, 10480–10487.
- [20] M. Yusuf, et al., *Cell Reports Physical Science* **2022**, *3*, 101145.
- [21] M. Sadd, S. Xiong, J. R. Bowen, F. Marone, A. Matic, *Nat. Commun.* **2023**, *14*, 854.
- [22] X. Xu, et al., *Adv. Energy Mater.* **2020**, *10*, 1–10.
- [23] A. Yang, et al., *ACS Energy Lett.* **2023**, *8*, 836–843.
- [24] M. C. Smart, B. L. Lucht, S. Dalavi, F. C. Krause, B. V. Ratnakumar, *J. Electrochem. Soc.* **2012**, *159*, A739–A751.
- [25] F. N. Jiang, et al., *Adv. Mater.* **2023**, *35*, 1–9.
- [26] V. Sharova, et al., *J. Power Sources* **2018**, *375*, 43–52.
- [27] E. C. Cengiz, J. Rizell, M. Sadd, A. Matic, N. Mozhzhukhina, *J. Electrochem. Soc.* **2021**, *168*, 120539.
- [28] J. R. Dahn, R. F. Moli, M. J. Spoon, *Phys. Rev. B* **1990**, *42*, 6424.
- [29] M. N. Obrovac, V. L. Chevrier, *Chem. Rev.* **2014**, *114*, 11444–11502.
- [30] S. Schweidler, et al., *J. Phys. Chem. C* **2018**, *122*, 8829–8835.

Manuscript received: January 31, 2024

Revised manuscript received: March 21, 2024

Accepted manuscript online: March 26, 2024

Version of record online: April 17, 2024